Functionalization of SBA-15 mesoporous silica for highly efficient adsorption of glutathione: Characterization and modeling studies

Laroussi Chaabane, Maria Nikolantonaki, Guy Weber, Igor Bezverkhyy, Remi Chassagnon, Ali Assifaoui, Frederic Bouyer

Functionalization of SBA-15 mesoporous silica for highly efficient adsorption of glutathione: characterization and modeling studies

Laroussi Chaabane[a,b,c*], Maria Nikolantonaki[b], Guy Weber[a], Igor Bezverkhyy[a], Remi Chassagnon[a], Ali Assifaoui[b,c], Frédéric Bouyer[a]**

[a] *Laboratoire Interdisciplinaire Carnot de Bourgogne, UMR 6303 CNRS-Université de Bourgogne Franche-Comté, 9 Avenue Alain Savary, BP 47 870, 21078 Dijon Cedex, France.*

[b] *UMR PAM Université de Bourgogne Franche-Comté /Institut Agro Sup Dijon, Institut Universitaire de la Vigne et du Vin, Jules Guyot, F-2100 Dijon, France.*

[C] *Department of pharmaceutical Technology, School of Pharmacy, Université de Bourgogne Franche-Comté, 7 Bd Jeanne d'Arc, 21079 Dijon, France.*

Corresponding authors:

*laroussi.chaabane@agrosupdijon.fr

**frederic.bouyer@u-bourgogne.fr

Highlights

- Adsorption of glutathione by functionalized SBA-15 materials was evaluated.
- Compared with pristine SBA-15-OH and SBA-15-SH, SBA-15-NH_2 show the highest adsorption capacity of glutathione.
- The adsorption capacity increases with temperature for SBA-15-OH and SBA-15-NH_2 but decreases for SBA-15-SH.
- The adsorption mechanism of glutathione is physisorption.
- The overall adsorption process is endothermic for SBA-15-OH and SCA-15-NH_2 and exothermic for SBA-15-SH.

Abstract

Background: Pristine SBA-15 and amine or thiol-functionalized SBA-15 materials were synthesized, characterized, and highlighted by studying the glutathione (GSH) adsorption process in aqueous solutions.

Methods: In this study, SBA-15 mesoporous materials were functionalized with 3-aminopropyltriethoxysilane (APTS) and (3-mercaptopropyl)triethoxysilane (MPTES) in order to introduce amine and thiol groups onto the surface by using a post-grafting method, respectively. For comparison, the SBA-15-based materials were used as adsorbents to further investigate the adsorption behaviour of GSH under various experimental conditions.

Significant Findings: To examine the underlying mechanism of the adsorption process, the kinetics of the GSH adsorption onto SBA-15-based adsorbents were fitted using pseudo-first order, pseudo-second order, Elovich, and Aharoni models. Adsorption isotherms showed that the Freundlich isotherm model was the most appropriate to simulate the adsorption of GSH molecules onto SBA-15-NH_2 adsorbent and the Langmuir isotherm model for the two other substrates. In addition, the adsorption thermodynamics confirmed the exothermic behaviour of GSH adsorption process onto the SBA-15-SH adsorbent. In contrast, the capture of GSH molecules by the SBA-15-OH and SBA-15-NH_2 adsorbents follows an endothermic reaction process. Finally, the adsorption nature of GSH onto SBA-15 adsorbents is classified as physisorption**.**

Keywords: *SBA-15 material, characterization, adsorption, glutathione, modeling.*

1. Introduction

Glutathione (GSH) is a tripeptide consisting of *L*-cysteine, glutamic acid, and glycine, and has two distinct structural features: a sulfhydryl group and a glutamyl linkage [1-3]. Furthermore, it is the major low molecular weight thiol present in mammalian and prokaryotic organisms acting mainly as regulator against oxidative stress, detoxification agent, and principal metabolite of sulfur and nitrogen metabolism [4, 5]. In addition, GSH manifests beneficial effects on human health due to its antioxidant, immune, and detoxifying properties, and it is considered a powerful, versatile, and essential self-generating defense molecule [6]. Historically, Cheynier et *al.*, were the first to extract GSH from grapes and conducted a study to analyze the GSH content of 28 different *Vitis vinifera* grape varieties [7]. The GSH content varied from 17 to 114 $mg.kg^{-1}$ between grape varieties [7]. However, the concentration of GSH in extracts containing protein, polypeptide, polysaccharide, pigment, and salts is so low that the separation and purification are very difficult [8]. In the past two decades, various methods have been applied to the separation and purification of GSH from the grape extracts, including ion exchange, capillary electrophoresis, nanofiltration, etc. [9-11]. However, all these methods have limitations such as energy or time consumption, being limited to small-scale production. The adsorption technique is regarded as an efficient, versatile, and simple technique for the separation and enrichment of molecules [12-14]. Nevertheless, to the best of our knowledge, there is currently no study devoted to the purification of GSH using mesoporous SBA-15 silica as adsorbent. As there are no studies assessing the effects of surface functionalization on the kinetics and adsorption properties of GSH, it would be valuable to study this effect to design an effective adsorbent, such as mesoporous materials, for the efficient adsorption of GSH.

The discovery of mesostructured silica materials in 1992 by Kresge *et al.* opened a new field of research in the design of porous solids [15-18]. As an example, SBA-15 (Santa Barbara Amorphous) materials, with a 2D hexagonal pore structure, have received much attention due

to specific characteristics such as high specific surface area, tunable pore size, nontoxicity, and biocompatibility [19-22]. Furthermore, compared with other meso-structured silica substrates such as MCM-41 materials, SBA-15 exhibits thick pore walls in the range 3.1 to 6.4 nm, providing high hydrothermal stability, suitable for various applications in aqueous media [23, 24]. These materials can also be easily functionalized by either co-condensation or post-grafting methods thanks to the presence of silanol groups and the large variety of silane molecules [25-31]. Tuning the surface chemistry of the pores opened new opportunities for developing mesoporous silica solids with very specific properties suitable for industrial applications such as adsorption processes, membrane separation, catalysis, drug delivery, or bio-sensing [32-37]. For example, Nguyen et *al.* reported that the functionalization of SBA-15 with amine groups results in an increase of the maximum adsorption capacity compared to that of the pristine SBA15 (for urea: 1644.7 $mg.g^{-1}$ compared to 950 $mg.g^{-1}$; for creatinine 181.7 $mg.g^{-1}$ compared to 56.5 $mg.g^{-1}$) [38]. Moreover, Moritz et *al.* modified SBA-15 and PHTS (Plugged Hexagonal Templated Silica) materials with propyl-sulfonic acid groups to study the adsorption of ticagrelor. They obtained a maximum adsorption capacity of 160 $mg.g^{-1}$ for SBA-15-$(CH_2)_3$-SO_3H, which was 2 times higher than PHTS-$(CH_2)_3$-SO_3H [39]. In addition, they demonstrated that 60% of active sites on the adsorbent surface were occupied by ticagrelor through chemical interactions between the mesoporous carrier and the drug molecule [39].

Analyzing and detecting organic molecules such as GSH in extract broth remains a challenge. Indeed, many analytical methods have been developed to determine the amount of reduced, oxidized, and total glutathione in grape extracts, and wine, but the preparation of samples and derivatization requires a great deal of time. Nikolantonaki et *al.* published a method to quantify GSH in wine-related systems, which does not require derivatization; high dosages of sodium bisulfate and 4-methylcatechol are used to inhibit oxidation of GSH, which has been allowing the routine analysis of large numbers of samples [2].

The present study is the first attempt to get information about the adsorption characteristics of GSH molecules onto the functionalized SBA-15. Therefore, these findings can provide insights for the future adsorption research of GSH molecules. For this purpose, the SBA-15 materials were synthesized and functionalized with amine and thiol groups by the post-synthesis method. The morphological and structural properties of the amine-functionalized SBA-15 (SBA-15-NH_2) and the thiol-functionalized SAB-15 (SBA-15-SH) were evaluated by FTIR, TGA, XRD, XPS, SEM, TEM, and BET techniques.

The influence of the surface chemistry of SBA15 was highlighted by comparing the GSH adsorption capacity of amine or thiol-functionalized SBA materials compared to SBA-15-OH adsorbent as a function of contact time, concentration of GSH, and temperature. The underlying mechanism of the adsorption process was analyzed by fitting the kinetic data with the pseudo-first order, pseudo-second order, Elovich and Aharoni models. Furthermore, the adsorption data were analyzed using the Freundlich and Langmuir approaches. Finally, the thermodynamic parameters such as enthalpy ($\Delta H°$), entropy ($\Delta S°$) and Gibb's free energy ($\Delta G°$) of GSH adsorption were systematically calculated from the experiments carried out between 283 and 313 K.

2. Experimental section

2.1. Chemicals and reagents

Triblock copolymer pluronic P123 surfactant [$(EO)_{20}(PO)_{70}(EO)_{20}$], MW=5800 $g.mol^{-1}$, Aldrich), tetraethylorthosilicate (TEOS, Aldrich), sodium hydroxide (NaOH, Aldrich), hydrochloric acid (HCl, Fisher Chemicals, 38%), ethanol (C_2H_5OH, Fisher Chemicals, 95.0 %), 3-aminopropyltriethoxysilane (APTS, Fisher Chemicals), (3-mercaptopropyl)triethoxysilane (MPTES, Fluorochem), sodium phosphate monobasic (NaH_2PO_4, Aldrich, ≥99.0 %), sodium phosphate dibasic (Na_2HPO_4, Aldrich, ≥99.0 %), Glutathione (GSH, $C_{10}H_{17}N_3O_6S$, Aldrich, ≥99.0 %), 4-methylcatechol (4-MeC, $C_7H_8O_2$, Aldrich ≥ 95.0 %), were used without further

purification. Chemical modification of SBA-15 mesoporous materials was achieved in dry toluene (homemade distillation). Ultrapure water (Resistivity = 18.25 MΩ cm) used to prepare standard solutions was obtained from a Milli-Q system (Milli-Q system, Elga, France).

2.2. Characterization

All SBA-15-based materials were characterized by Fourier transform-infrared spectroscopy (FTIR) using a Bruker Equinox 55 spectrometer equipped with a DTGS detector. The FTIR spectra were recorded using KBr pellets prepared by mixing a small amount of material (~1-2 mg) with 200 mg of KBr. Each sample was scanned 100 times between 4000 to 400 cm^{-1} with a resolution of 4 cm^{-1}. The decomposition of organic moities grafted onto the SBA-15-based materials was characterized by thermogravimetry (TA instruments, Discovery, USA); the samples were dried at 100 °C for one hour and heated under air flow between 100 and 800 °C with a heating rate of 10 $°C.min^{-1}$. The surface morphologies were identified using high-resolution scanning electron microscopy (HR-SEM) images that were obtained by a commercial FEI Quanta 250 FEG at a typical accelerating voltage of 10 kV. The mesostructure of SBA-15 materials was characterized using a Transmission Electron Microscope (TEM, JEM2100, JEOL; Japan) operating at 200 kV with very low illumination to avoid the destruction of material under the electron beam. X-ray photo-electron spectroscopy (XPS, Thermo Fisher Scientific, USA) analyses were performed on a XPS PHI 5000 Versa-Probe using a spectrometer with a monochromatized Al K_α radiation (1486.7 eV). The binding energies were calibrated from the C1s, binding energy set at 284.8 eV. The structure of the pristine and functionalized SBA-15 materials was evaluated using low-angle powder X-ray Diffraction (PXRD, Bruker D8, USA) patterns collected on an X-ray diffractometer, and equipped with Cu K_α radiation at 35 kV and 35 mA. The textural properties of the SBA-15-based materials were determined by N_2 adsorption/desorption isotherms at 77K using a Micromeritics ASAP 2020 setup (Micromeritics Instrument, Nocross, GA). All samples were

previously degassed at 353 K under vacuum to ensure a dry surface, free of any loosely bound adsorbed species. Specific surface areas (S_{BET}) were calculated using the Brunauer-Emmett-Teller (BET) method in the relative pressure range 0.06 - 0.25. The pore-size distribution was obtained from the adsorption branch of the nitrogen isotherms following the Barrett-Joyner-Halenda (BJH) method. The total pore volume (V_m) was defined at P/P_0= 0.95. The concentration of Glutathione (GSH) with 4-methylcatechol (4-MeC, oxidizing agent) solutions were measured using an ultrahigh pressure liquid chromatography (Dionex Ultimate 3000, Thermo Fischer Scientific, Waltham, MA USA) coupled to a MaXis plus MQ ESI QqTOF mass spectrometer (Bruker, Bremen, Germany).

2.3. Synthesis of the SBA-15-OH mesoporous material

The SBA-15-OH mesoporous material was synthesized according to the method reported by Yuan et *al.* [40]. In a typical reaction, 3.0 g of Pluronic P123 was completely dissolved in 80 mL of hydrochloric acid solution (HCl, 2M) by continuously stirring at 313 K; then 6.24 g of tetraethylorthosilicate (TEOS) was added dropwise to the homogenous solution. The resultant mixture was kept under a slow stirring rate at 313 K for 24 h and then was subsequently transferred to a Teflon autoclave to be heated at 373 K for another 24 h. At the end of the condensation process, the white precipitated solid was collected by centrifugation (10 000 *g*, 10 min, 293 K), washed with deionized water several times, and finally dried under vacuum at 333 K overnight. Then, the white product was calcined under airflow (0.20 $mL.min^{-1}$) at 823 K for 6 h (heating rate 1 $K.min^{-1}$) to eliminate the organic template. Without further modification, the sample was referred to as SBA-15-OH.

2.4. Post-grafting of the SBA-15-OH material

The SBA-15-OH mesoporous material was modified with amine or thiol groups using a post-grafting method according to a previous report with some modifications [15]. Before

surface functionalization, 0.200 g of SBA-15-OH was dried at 373 K for 8 h to remove physisorbed water. Afterward, the sample was kept under N_2 flow and then dispersed in 10.0 mL of anhydrous toluene. Thereafter, 8.5 mmol of 3-aminopropyltriethoxysilane (APTS) or (3-mercaptopropyl)triethoxysilane (MPTES) was added dropwise into the SBA-15-OH suspension for functionalization with amine or thiol groups, respectively (**Scheme 1**).

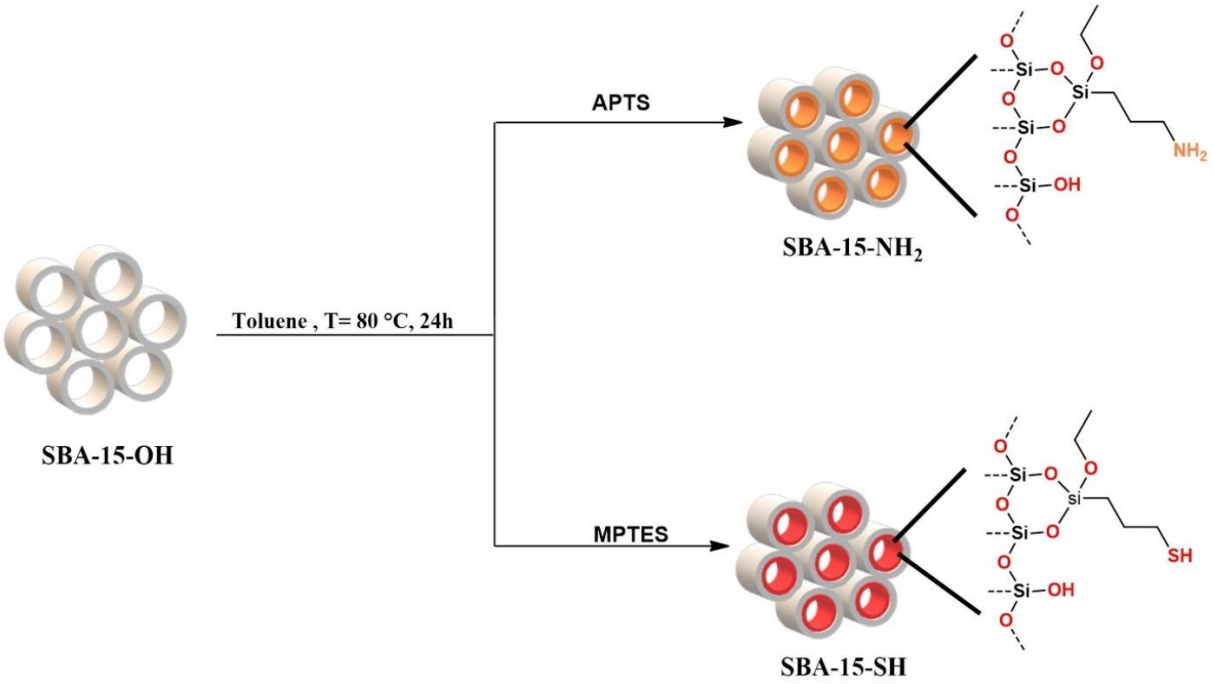

Scheme 1. Functionalization of SBA-15-OH material with APTS or MPTES.

The mixture was stirred under reflux at 353 K for 24 h. At the end of the reaction, the functionalized samples were collected by centrifugation (10 000 g, 20 min, 293 K), washed with ethanol several times to remove the unreacted and physically adsorbed reagents and dried under vacuum at 353 K overnight. Finally, the samples functionalized with MPTES and APTS were referred to as SBA-15-SH and SBA-15-NH_2, respectively.

2.5. Adsorption studies

The adsorption capacities of glutathione (GSH) onto SBA-15-based adsorbents were measured considering several parameters: contact time, initial glutathione (GSH) concentration, and temperature. For all samples, the pH solution was kept constant at 7.0 using Clark-Lubs buffer solutions (0.1 M HCl, 0.1 M NaOH). This operating condition was encouraged toward the development of an eco-friendly adsorption process, *i.e*., elimination of the use of acid/base and excessive energy. 50 mg of adsorbent was added into a 10 mL amber glass bottle containing 4.0 mL of 1.25 $mg.mL^{-1}$ GSH aqueous solution, and the resulting suspension was strongly stirred at room temperature (298 K) for 24 h. Then, the supernatant was collected by centrifugation (11000 g, 15 min, 293 K). Finally, the initial and equilibrium concentration of GSH in each solution was measured by UPLC coupled to a mass spectrometer according to the protocol proposed by Nikolantonaki *et al.* [2].

To investigate the kinetics behavior of the three tested adsorbents (SBA-15, SBA-15-NH_2, and SBA-15-SH), GSH adsorption capacities were examined over 30-600 min of time range at 298 K. In addition, adsorption isotherm experiments were carried out with the same amount of sample (50 mg) and were performed at 283 K, 295 K, 303 K, and 313 K in the presence of various GSH concentrations from 1.25 to 15 $mg.mL^{-1}$ and the adsorption thermodynamic parameters were evaluated. The adsorption capacity Q_e ($mmol.g^{-1}$) and the percentage of adsorption efficiency E_{Ads} (%) at the equilibrium state were calculated by using **Eqs. (1)** and **(2)**, respectively [41]:

$$Q_e = \frac{V(C_0 - C_e)}{m} \quad (\mathbf{1})$$

$$E_{Ads} = \frac{(C_0 - C_e)}{C_0} \times 100 \quad (\mathbf{2})$$

where C_0 and C_e are the initial and equilibrium concentrations of GSH in solution, respectively, V is the volume of the solution and m the weight of the adsorbent.

For the kinetic study of GSH adsorption on the SBA-15-based adsorbents, the adsorption capacity Q_t at a time t was calculated using **Eq. (3)** [41]:

$$Q_t = \frac{V(C_0 - C_t)}{m} \quad (3)$$

where C_t is the residual glutathione (GSH) concentration in solution at time t.

3. Results and discussion

3.1. Characterization of SBA-15-based materials

The textural properties such as specific surface area (S_{BET}), pore volume (V_p), pore size (D_p), and pore wall thickness (t_{wall}) of non-functionalized and functionalized SBA-15 mesoporous materials are provided in **Table 1.**

Table 1. Structural and textural characteristics of pristine and functionalized SBA-15 mesoporous materials determined by X-ray diffraction (†) and N_2 adsorption-desorption isotherms measurements (*).

Sample	S_{BET}*(m^2/g)[a]	V_p*(cm^3/g)[b]	D_p*(nm)[c]	d_{100}†(nm)[d]	a_0†(nm)[e]	t_{wall}†(nm)[f]
SBA-15-OH	689	1.01	6.16	10.46	12.08	5.92
SBA-15-NH_2	214	0.33	4.99	10.68	12.33	7.34
SBA-15-SH	426	0.64	5.72	10.56	12.15	6.43

[a]: specific surface area calculated in the relative pressure range between 0.06 and 0.25.
[b]: total pore volume determined at $P/P_0 = 0.95$. [c]: pore diameter calculated from adsorption branch using the Barrett-Joyner-Halenda (BJH) model.
[d]: *d*-spacing calculated from the (100) diffraction peak.
[e]: unit cell parameter calculated using $a_0 = (2d_{100}/\sqrt{3})$.
[f]: pore wall thickness calculated using the equation $T_{wall} = a_0 - D_p$.

As expected, all samples exhibit type IV adsorption isotherms **(Fig. 1)** with an H1 hysteresis loop, characteristic of mesoporous materials with a narrow distribution of the pore size [42]**.**

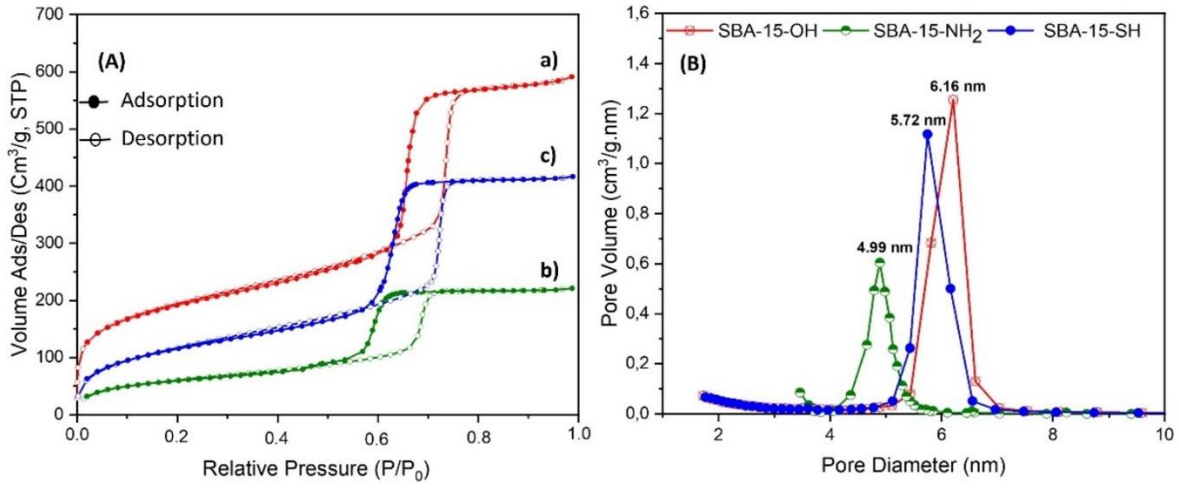

Fig. 1. (A) N_2 adsorption-desorption isotherms at 77 K and **(B)** Pore size distribution of **(a)** SBA-15-OH**, (b)** SBA-15-NH_2, and **(c)** SBA-15-SH.

The specific surface areas of SBA-15-OH, SBA-15-NH_2, and SBA-15-SH were 689, 214, and 426 $m^2.g^{-1}$, respectively **(Table 1)**. The decrease in the specific surface area (S_{BET}) for functionalized SBA-15 mesoporous materials was ascribed to the presence of organosilanes in the pores. This interpretation was also confirmed by the lower pore volume (V_p) and pore size (D_p) of functionalized SBA-15 materials. Furthermore, the decrease in the specific surface area (S_{BET}), pore volume (V_P), and pore size (D_p) was larger for SBA-15-NH_2 than for SBA-15-SH **(Table 1)**. This behavior may be ascribed to the more basic properties of amine groups. It results in a higher chemical reactivity of APTES and consequently a higher grafting ratio of amine groups onto mesoporous SBA-15 material, as proposed by Zhao et *al.* [31].

To describe the structure of the mesoporous materials, XRD patterns of SBA-15 materials were measured then, the unit cell parameters (a_0) and the d_{100} values were calculated. The results are summarized in **Table 1**.

All the materials exhibit three well-resolved peaks, indexed as (100), (110), and (200) indicating of a 2D-hexagonal symmetry *(P6mm)* with highly well-ordered mesostructures **(Fig. S1)**.

In addition, the larger wall thickness (t_{wall}) and the smaller pore size of functionalized materials compared to SBA-15-OH confirm the successful grafting of organic functional groups inside the mesopores.

The scanning electron microscopy (SEM) and the transmission electron microscopy (TEM) images further confirmed the results of the small-angle XRD patterns, and the narrow pore size distribution obtained from nitrogen adsorption-desorption isotherms. For example, in **Fig. S2a** the SEM image of the SBA-15-OH material shows that the synthesized powder is composed of agglomerates of size ranging from approximately 0.1 to about 1.1 µm. In addition, the TEM images **(Figs. S3a and S3b)** clearly demonstrate the internal structure of SBA-15-OH with parallel channels along the (110) direction, as discussed by Yuan et *al.* [40]. Consequently, the qualitative studies demonstrate that the SBA-15 materials have highly ordered 2-D hexagonal mesostructures. To confirm the presence of amine and thiol functional groups onto the SBA-15-OH materials, the pristine and the grafted materials were analyzed by Fourier transform-infrared spectroscopy (FTIR) **(Fig. 2)**.

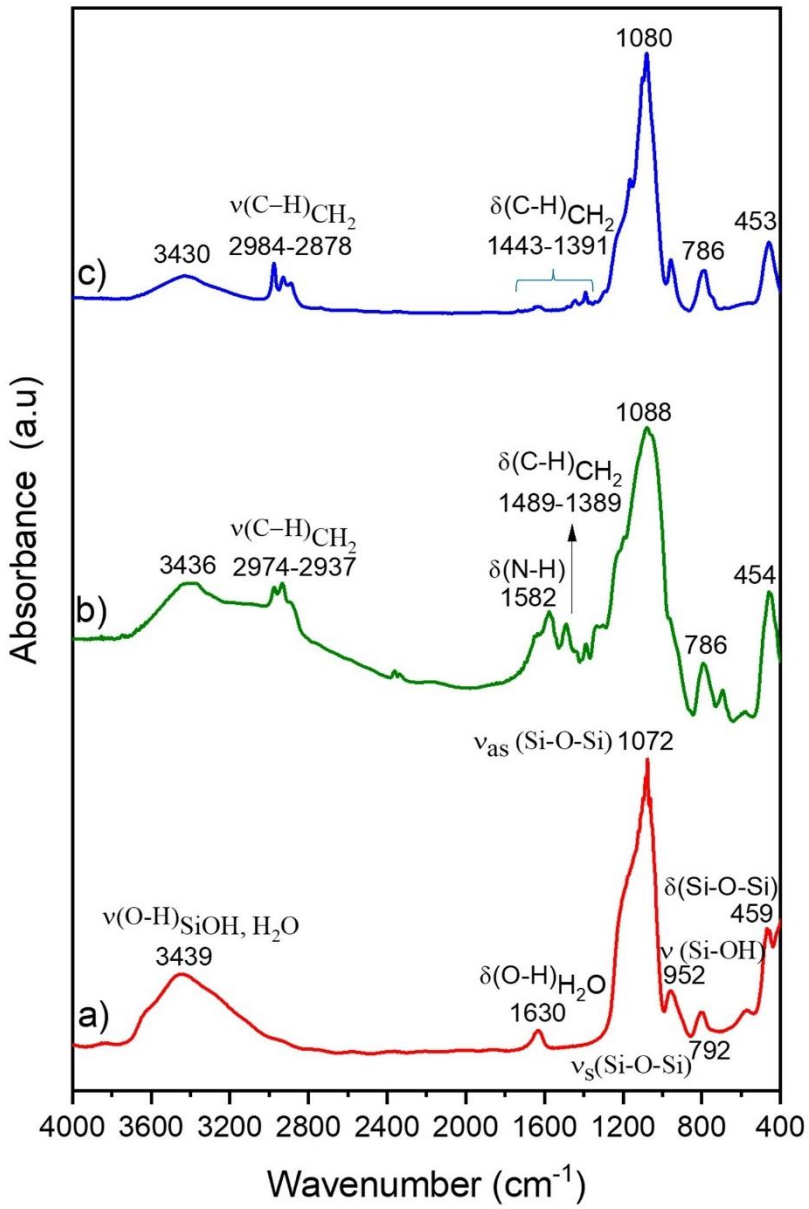

Fig. 2. FTIR spectra of **(a)** SBA-15-OH, **(b)** SBA-15-NH_2, and **(c)** SBA-15-SH.

As expected, all the FTIR spectra exhibit similar characteristic bands of silica network, including absorption bands in the range 1072-1088 cm^{-1} and 786-792 cm^{-1} corresponding to the asymmetric and symmetric stretching vibrations of Si-O-Si bonds, respectively [43]. For SBA-15-OH, O-H bending vibration of physically adsorbed moisture and O-H stretching vibration of molecular water hydrogen bounded to each other and to Si-OH groups can be observed at 1630 and 3439 cm^{-1}, respectively. The intensity of the absorption band located at 952 cm^{-1}

corresponding to the stretching vibration of free silanol (Si-OH) was decreased for SBA-15-NH_2 and SBA-15-SH, which confirms the successful grafting of organosilanes [43]. The presence of absorption bands in the range 2800-3000 cm^{-1}, characteristic of C-H stretching vibrations confirms the presence of the organic moieties. The peak at 1582 cm^{-1}, due to the vibration of N-H bending groups, confirms the presence of amine groups in the SBA-15-NH_2 sample. In addition, the S-H stretching vibration was a weak band at 2573 cm^{-1}, proving that MPTES was successfully anchored on the silica surface **(Fig. S4).**

XPS analysis was applied to study the surface composition of SBA-15-SH **(Fig. 3)**.

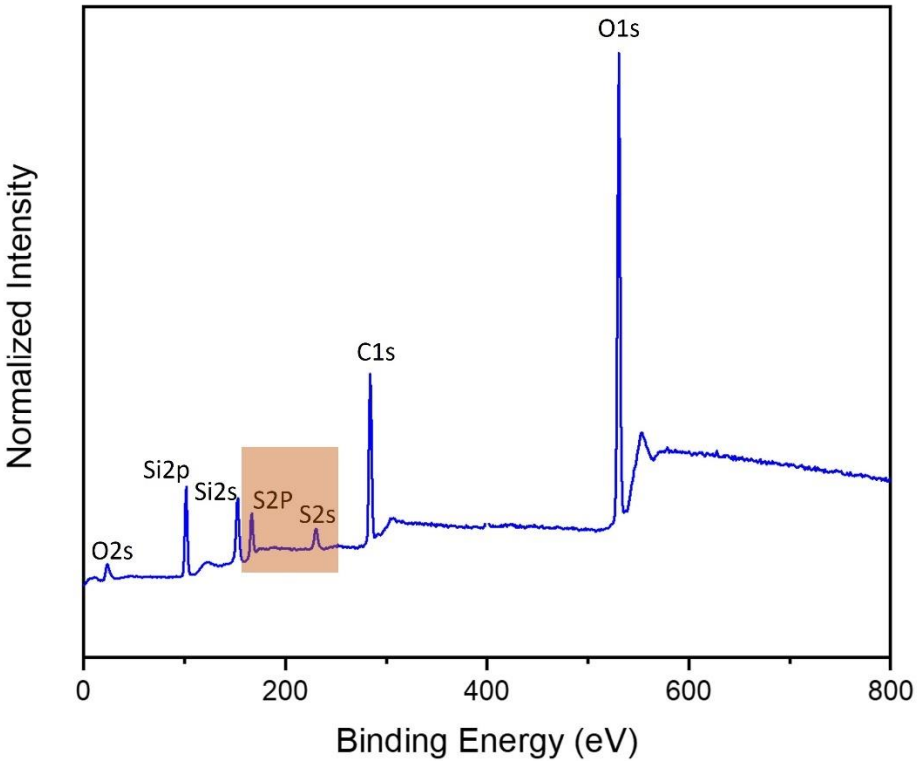

Fig. 3. Survey XPS spectrum for SBA-15-SH.

Fig. 3. shows that the surface of SBA-15-SH material contains C, O, Si, and S and no other elements. Particularly, the presence of two peaks at 230 and 163 eV can be ascribed to S2s, and S2p, respectively, characteristic of thiol groups **(Fig. 3)** [44]. Besides, the absence of a peak at 168 eV suggests the absence of sulfur oxidation during the post-grafting process.

The thermal behavior of the pristine and the functionalized SBA-15 mesoporous materials was evaluated by TGA under airflow **(Fig. 4)**. The TGA curve of SBA-15-OH material **(Fig. 4a)** shows only a slight weight loss between 200 and 800 °C of about 1.0 %.wt, due to the dehydroxylation of silica **(Fig. S5)**. The TGA curves for SBA-15-NH_2 **(Fig. 4b)** and SBA-15-SH **(Fig. 4c)** samples exhibit different behaviors due to the decomposition of silane moieties. From the difference of weight losses at 800 °C, the grafting densities of the functionalized materials were calculated, i.e. 3.94 and 1.38 mmol.g^{-1}, respectively **(Table S1 in supporting information).**

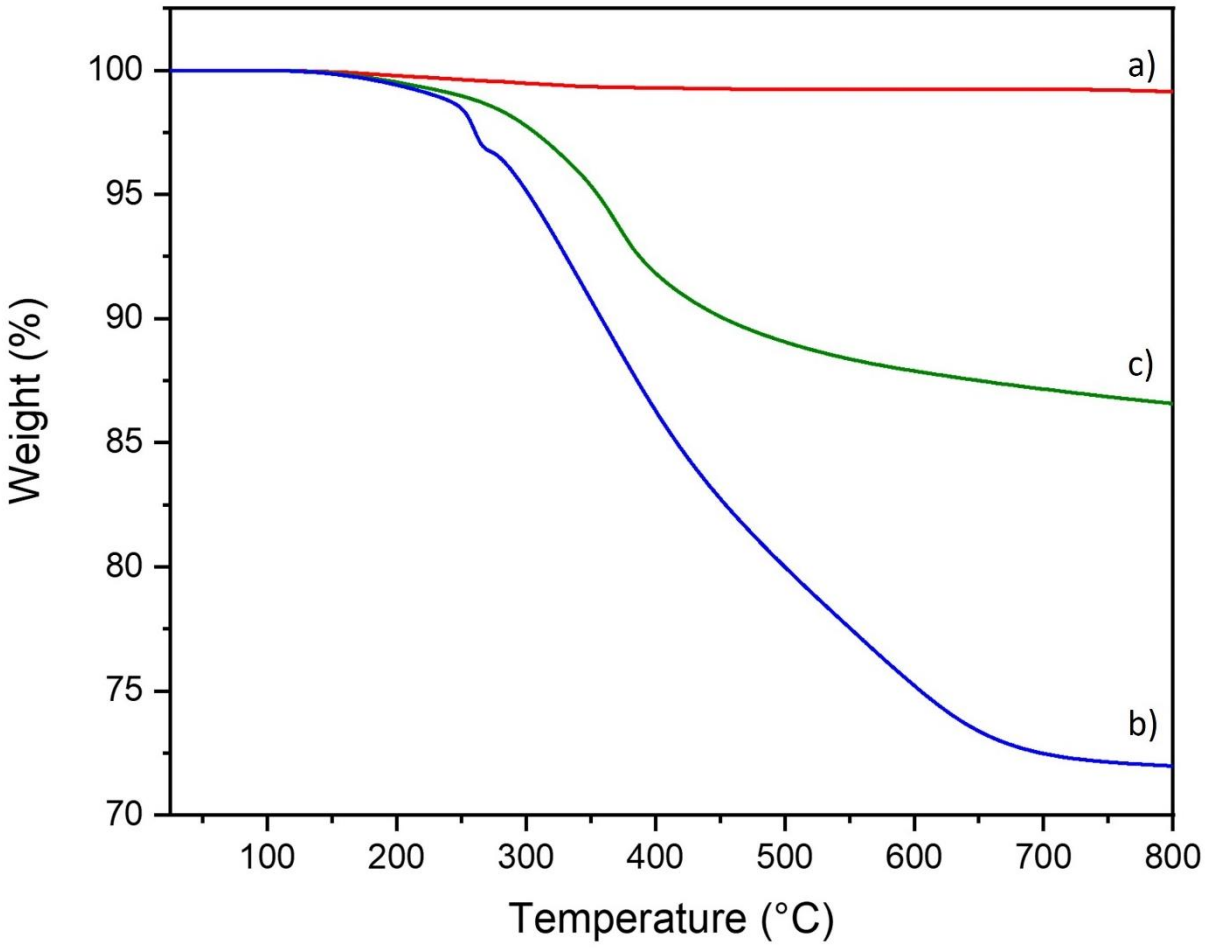

Fig. 4. TGA analysis of **(a)** SBA-15-OH, **(b)** SBA-15-NH_2, and **(c)** SBA-15-SH.

3.2. Effect of experimental conditions on glutathione (GSH) adsorption

3.2.1. Effect of contact time on the maximum adsorption capacities

In order to determine the equilibrium time for the adsorption of GSH by SBA-15-based adsorbents, the adsorption experiments were carried out at different contact times in the range 30-3600 min and the concentration of mesoporous materials was fixed at 12.5 mg.mL^{-1} **(Fig. 5)**.

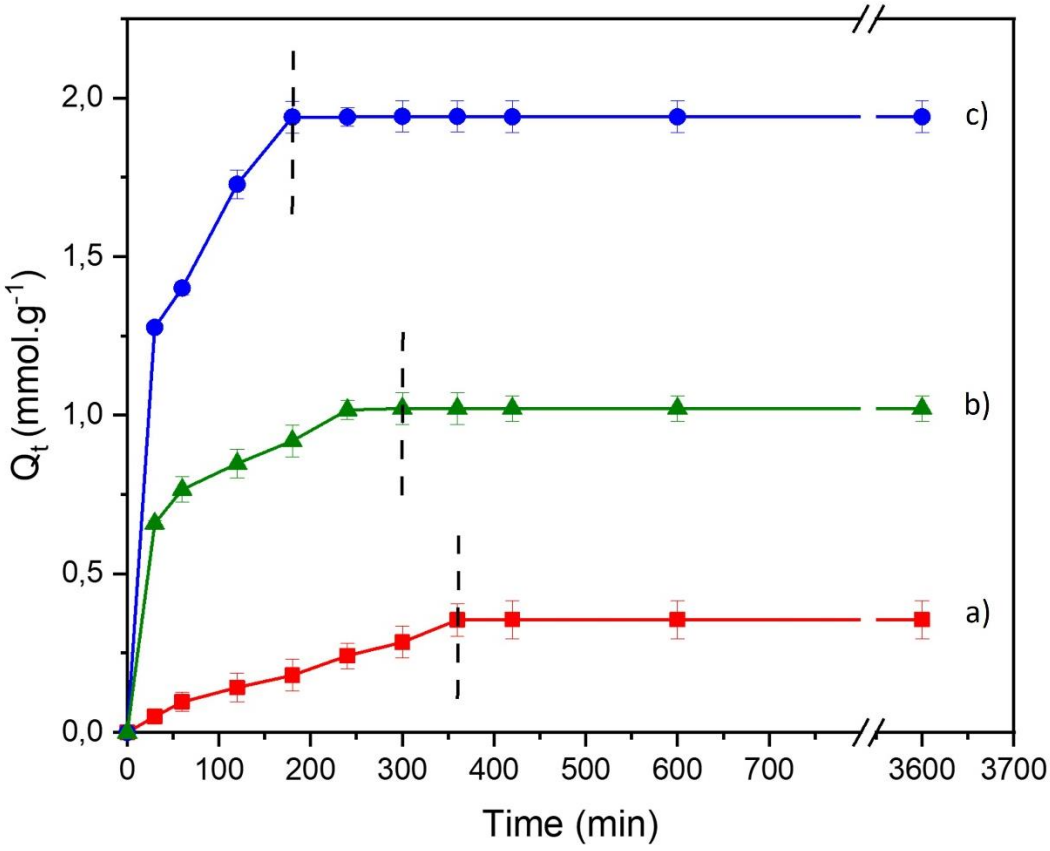

Fig. 5. Effect of contact time on the adsorption of GSH by **(a)** SBA-15-OH, **(b)** SBA-15-SH, and **(c)** SBA-15-NH_2. **Experimental conditions**: [GSH] = 10 mg.mL^{-1}, [Adsorbent]= 12.5 mg.mL^{-1}, pH = 7, and T = 298 K. The error bars correspond to one standard deviation n = 2.

Fig. 5 clearly shows that the adsorption process of GSH molecules onto SBA-15-based adsorbents is relatively fast and takes less than 6 hours whatever the adsorbent. This behavior can be explained by the high surface area and the high number of adsorption sites. The contact

time required to reach equilibrium depends on the functional groups: 360 min for SBA-15-OH, 300 min for SBA-15-SH, and 180 min for SBA-15-NH_2.It is noteworthy to observe that the time needed to reach equilibrium is faster for SBA-15-NH_2 than SBA-15-OH and SBA-15-SH. Moreover, the amine-grafted silica show the highest adsorption capacity of GSH molecules (1.94±0.05 mmol.g^{-1}). This could be attributed to the greater availability of adsorption sites onto SBA-15-NH_2, as well as the higher grafting density of aminosilane groups.

3.2.2. Effect of initial GSH concentration on the equilibrium adsorption capacities

Fig. 6 presents the adsorption capacity, Q_e, and the adsorption efficiency E_{Ads} (%) of glutathione (GSH) in the presence of SBA-15-OH, SBA-15-NH_2, and SBA-15-SH adsorbents after 24 h of mixing. In those conditions, all samples were at equilibrium. For all materials, the initial GSH concentration ranged from 1.25 to 15 mg.mL^{-1} with keeping constant all the other parameters.

At low GSH initial concentration, the equilibrium adsorption capacities of SBA-15-based adsorbents, Q_e, increased almost linearly with increasing the initial GSH concentration because of strong interactions between GSH molecules and the active adsorption sites onto the adsorbents.

At high GSH concentration, typically above 10 mg.mL^{-1}, the equilibrium adsorption capacities of the mesoporous materials become approximately constant due to the saturation of the active adsorption sites onto the surface of the adsorbents. Unless otherwise stated, a GSH concentration of 10 mg.mL^{-1} will be used for the following experiments.

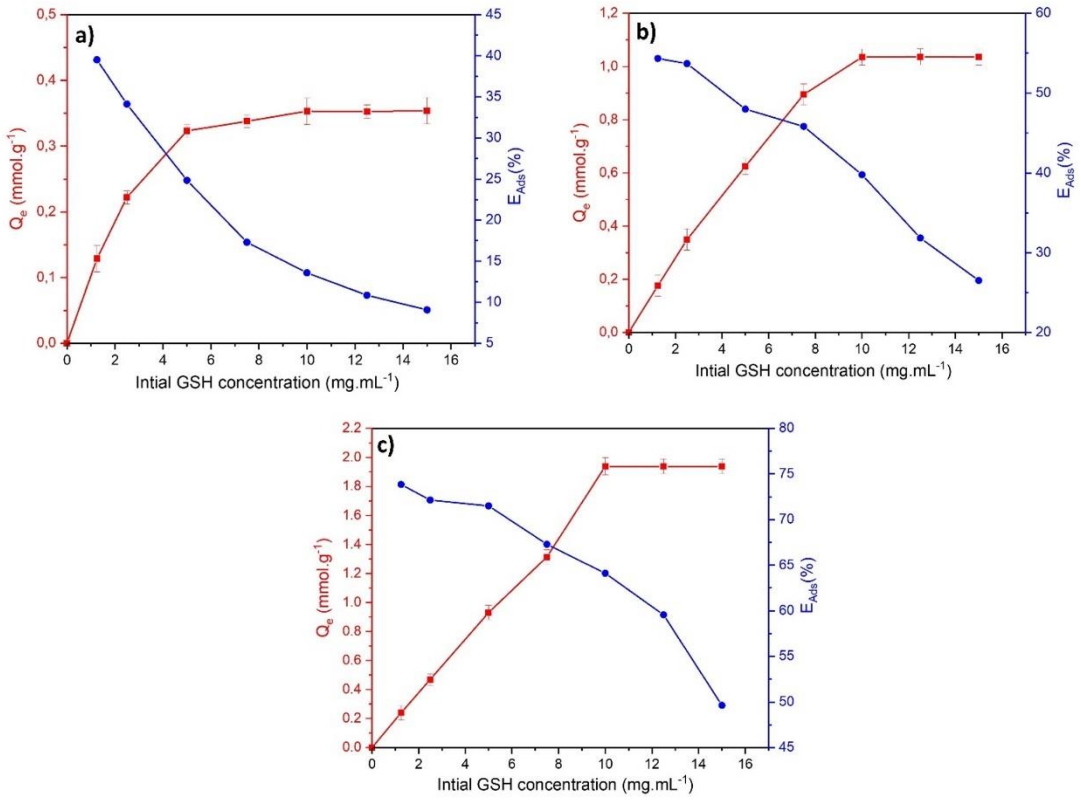

Fig. 6. Effect of initial concentration on the adsorption of GSH by **(a)** SBA-15-OH, **(b)** SBA-15-SH, and **(c)** SBA-15-NH_2. **Experimental conditions**: [Adsorbent]= 12.5 mg.mL $^{-1}$, pH = 7, T= 298 K, t = 24 h. The error bars correspond to one standard deviation n = 2.

The maximum amount of GSH adsorbed ($Q_{e,max}$) at the plateau, is 0.32, 1.94 and 1.05 mmol.g^{-1} for SBA-15-OH, SBA-15-NH_2 and SBA-15-SH respectively. This result indicates that the SBA-15-NH_2 adsorbent exhibits the highest adsorption capacity for GSH. Moreover, if compared to the grafting density of the silanes (**Table S1**), the maximum adsorption capacities are 0.48 mmol GSH/mmol NH_2 group and 0.76 mmol GSH/mmol SH group suggesting a higher affinity of GSH molecules for thiol groups on grafted-SBA-15 materials.

In addition, the adsorption efficiency for SBA-15-OH, SBA-15-NH_2, and SBA-15-SH adsorbents systematically decreased with increasing the initial GSH concentration from 1.25 to 15 mg.mL^{-1}, from 40 to 9% for SBA-15-OH, from 74 to 50% for SBA-15-NH_2 and from 54 to 27% for SBA-15-SH.

3.3. Adsorption kinetics

To understand the mechanism and the dynamic of adsorption of GSH molecules onto SBA-15-based adsorbents, the experimental data were analyzed by suitable kinetic models such as the pseudo-first order kinetic (PFO) model [45], the pseudo-second order (PSO) kinetic model [46], the Elovich kinetic model [47], and the Aharoni kinetic model [48,49]. A short description of these models is provided in supporting information (**see text section 2**).

The evaluation of the kinetic parameters obtained from the linear fittings of PFO **(Fig. S6)**, PSO **(Fig. S7)**, Elovich, and Aharoni models are presented in **Table 2** together with the error functions of the correlation coefficient (R^2) and the standard deviation Δ_q(%).

Table 2. Kinetic parameters calculated from the PFO, PSO, Elovich and Aharoni models for the adsorption of GSH molecules onto SBA-15-OH, SBA-15-NH_2, and SBA-15-SH at T = 298 K.

		Adsorbent		
		SBA-15-OH	**SBA-15-NH_2**	**SBA-15-SH**
Kinetic model	**Parameters**			
Pseudo first order (PFO)	**$Q_{e,\,exp}$ (mmol.g^{-1})**	0.36±0.01	1.94±0.07	1.02±0.01
	$Q_{e,\,calc}$ (mmol.g^{-1})	0.37±0.02	1.52±0.10	0.95±0.21
	$k_f \times 10^2$ (min^{-1})	0.51±0	1.79±0.01	1.71±0.01
	R^2	0.97	0.93	0.86
	Δ_q (%)	1.89	7.22	14.45
Pseudo second order (PSO)	**$Q_{e,\,exp}$ (mmol.g^{-1})**	0.36±0.01	1.94±0.07	1.02±0.01
	$Q_{e,\,calc}$ (mmol.g^{-1})	0.39±0.04	2.02±0.08	1.07±0.05
	$k_s \times 10^2$ (g.mmol^{-1}.min^{-1})	0.49±0.01	4.09±0.01	3.23±0.01
	R^2	0.91	1	1
	Δ_q (%)	>100	1.25	1.38
Elovich model	**A (mmol.g^{-1}.min$^{-1/2}$)**	0.01±0.07	1.60±0.19	0.66±0.07
	B (g.mmol^{-1})	8.42±0.01	3.96±0.04	7.38±0.01
	R^2	0.92	0.87	0.94
	Δ_q (%)	10.70	3.62	1.26
Aharoni model	**$k_A \times 10^4$ (mL.g^{-1}.L^{-1})**	0.019±0.07	2.29±0.05	1.43±0.02
	α	0.73±0.034	0.24±0.029	0.19±0.010
	R^2	0.99	0.97	0.99
	Δ_q (%)	1.46	0.99	0.013

For SBA-15-OH adsorbent, the PFO model is more appropriate than the PSO model to describe the adsorption process of GSH considering that the calculated equilibrium adsorption

capacity ($Q_{e,\,calc}$, mmol.g^{-1}) is much closer to the experimental data ($Q_{e,\,exp}$, mmol.g^{-1}). This is supported by the larger value of the correlation coefficient (R^2) and the smaller standard deviation (Δ_q (%)) of the PSO model. On the contrary, the adsorptions of GSH onto SBA-15-NH_2 and SBA-15-SH are better described by the PSO model. In addition, the SBA-15-NH_2 adsorbent exhibits a higher adsorption rate constant (k_s) than SBA-15-OH, and SBA-15-SH adsorbents and this behavior may be explained by the higher grafting density of amine groups.

Scheme 2 summarizes the interactions between GSH molecules and the surface of SBA-15-NH_2 and SBA-15-SH at pH = 7.

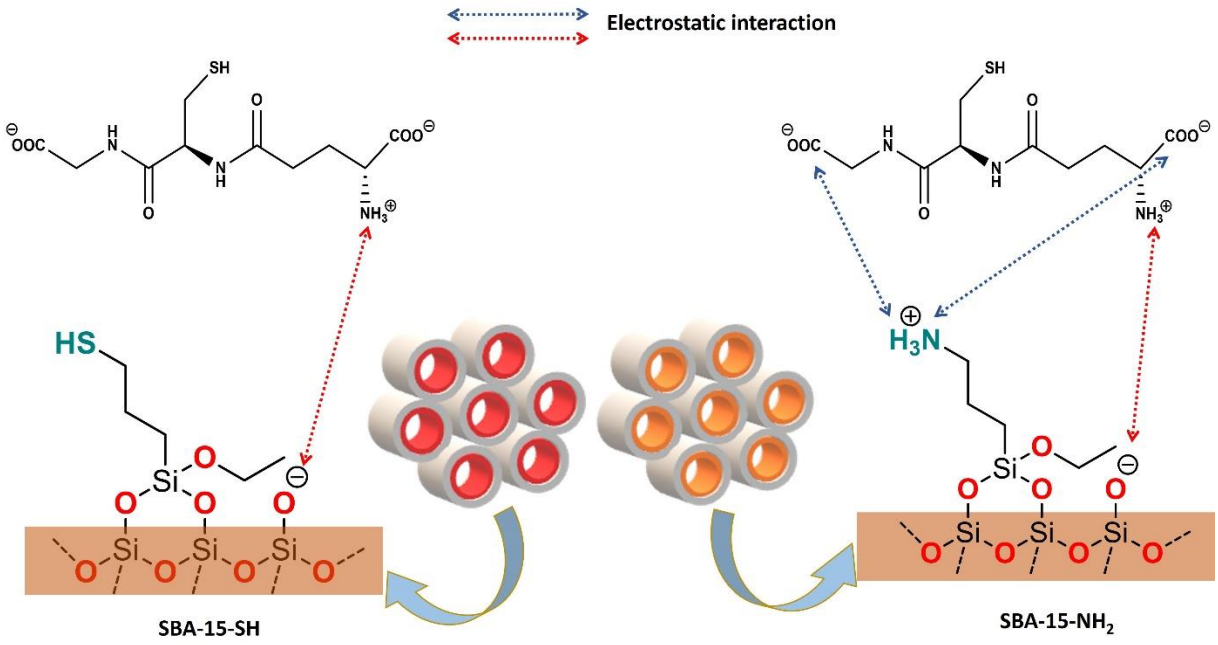

Scheme 2. Illustrative scheme of the cooperative adsorption mechanism between a GSH molecule and the active adsorption sites onto SBA-15-NH_2 and SBA-15-SH adsorbent.

First, considering the pK_a values of GSH (pK_{a1}(R_1-COOH) = 2.12; pK_{a2} (R_2-COOH) = 3.59; pK_{a3} (R_3-SH) = 8.75; pK_{a4} (R_4-NH_2= 9.20)) [50] and the pK_a value of the amine groups of APTES (10.37), the adsorption process is based on electrostatic interactions between (i) the ammonium group of GSH and one silanolate group of SBA-15-NH_2 and (ii) the two carboxylate (R_1-COO^- or R_2-COO^-) groups of GSH and the surface ammonium group of SBA-15-NH_2.

Then, the smaller adsorption rate affinity of GSH molecules towards SBA-15-SH, may be explained the disorderliness in the complex SBA-15-SH/GSH during the adsorption process or the formation of a novel bond of disulfide between a thiol group onto SBA-15-SH adsorbent and thiol groups of GSH molecules.

The Elovich model is also used to describe the nature of the adsorption process when the surface of the adsorbent is heterogeneous [47]. The parameters of the linear fitting results are listed in **Table 2**. The initial rate adsorption constant "A" increases in the order SBA-15-OH< SBA-15-SH<SBA-15-NH_2. Meanwhile, the rate desorption constant "B" decreases in the order SBA-15-OH>SBA-15-SH>SBA-15-NH_2, that is consistent with the higher adsorption rate affinity of GSH towards the heterogeneous active adsorption sites on functionalized materials and the higher grafting density of amine groups.

Aharoni's kinetic model is also tested to explore the possibility for the GSH molecules to be adsorbed within the pores of SBA-15 adsorbents. The Aharoni parameters as well as the R^2 and Δ_q (%) values, are listed in **Table 2**. The diffusion constant k_A decreases according to the following order: SBA-15-NH_2>SBA-15-SH>SBA-15-OH. This result suggests that the rate-controlling step is the pore diffusion and that the nature of the functional groups located onto the pore surface of SBA-15-based adsorbents play a significant role in the progress of the reactions. Moreover, the low values of the rate constants α (α<1 for all adsorbents) indicate that pore diffusion is a predominant mechanism during the adsorption process of GSH molecules.

3.4.Adsorption isotherms

Fig. 7 displays the adsorption isotherms of GSH onto the SBA-15-based materials at temperatures ranging from 283 to 313 K.

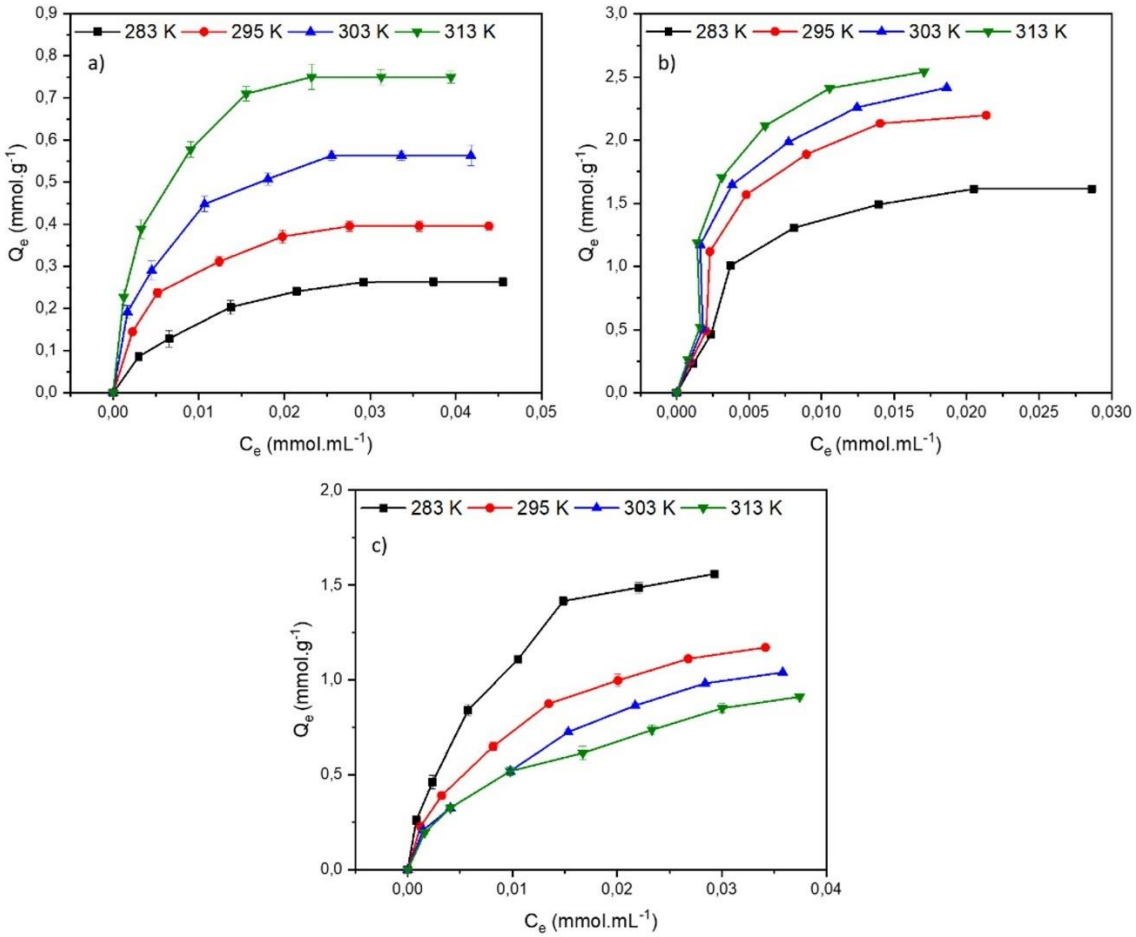

Fig.7. Effect of temperature on the adsorption of GSH onto **(a)** SBA-15-OH, **(b)** SBA-15-NH_2, and **(c)** SBA-15-SH adsorbents. The error bars correspond to one standard deviation n = 2.

It was found that the adsorption capacities of GSH onto the SBA-15-OH and SBA-15-NH_2 adsorbents increase with an increase in temperature. In contrast, at constant equilibrium concentration, the adsorption capacity of GSH onto the SBA-15-SH adsorbent decreases with an increase in temperature, which is mainly due to the low energy attraction between GSH molecule and thiol group. A comparison of the fitting of the experimental data with the adsorption isotherms of the Freundlich (**section 3, Table S2 in supporting information**) [50]

and Langmuir (**section 3, Table S3 in supporting information**) [51, 52] models is presented in **Fig. 8**.

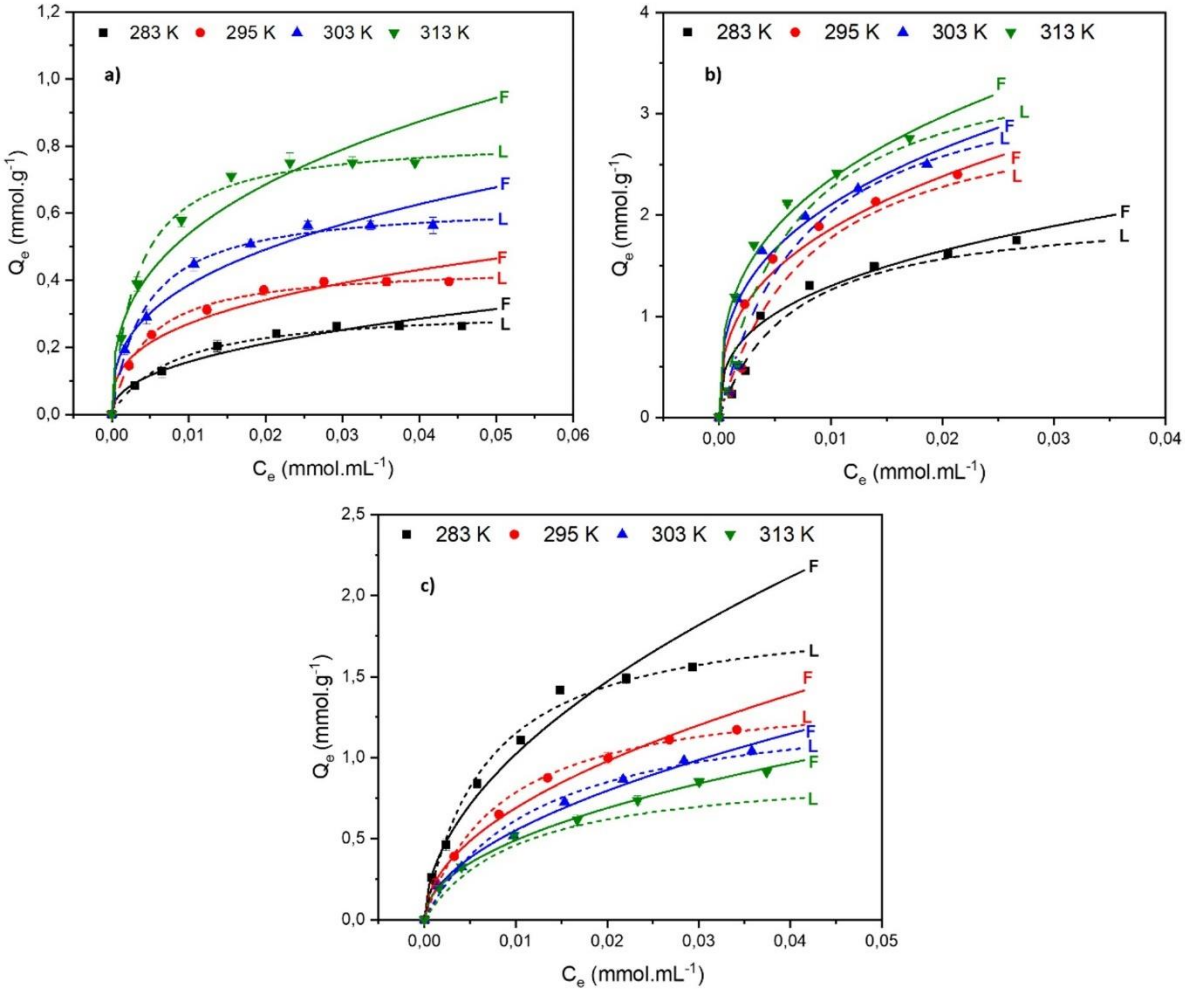

Fig.8. Comparison of the predicted adsorption isotherms and the experimental adsorption data for GSH onto **(a)** SBA-15-OH, **(b)** SBA-15-NH_2, **(c)** SBA-15-SH adsorbents at 283, 295, 303 and 313 K, according to the Freundlich **(F)** and Langmuir **(L)** models.

The Freundlich isotherm model is more appropriate than the Langmuir model to fit the experimental adsorption data for SBA-15-NH_2 adsorbent than for those of SBA-15-OH and SBA-15-SH adsorbents, as can be seen from the higher values of correlation coefficient (R^2) and the least values of standard deviation Δ_q (%) (**Tables S2-3**) and **Fig. 8**. This isotherm model indicated that the adsorption process of GSH onto the SBA-15-NH_2 adsorbent might be

described by multilayer adsorption. Moreover, all n values for the SBA-15-NH_2 adsorbent were found to be above 1, suggesting that the adsorption process occurs on heterogeneous active adsorption sites. Further, the highest parameter K_F represents the adsorption capacity Freundlich values, which are observed at 313 K for SBA-15-NH_2. The results suggest that different amino groups onto adsorbents exhibit different behavior that are temperature dependent when combining with GSH molecules.

Fig. 8 clearly shows that the Langmuir isotherm fits well the adsorption of GSH on the SBA-15-OH and SBA-15-SH adsorbents suggesting that monolayer surface coverage was achieved in the studied concentration domain and that the adsorption active sites on these two adsorbents may be considered as homogeneous (see also the values of the correlation coefficients (R^2) and those of the standard deviations Δ_q (%) given in **Table S3 in supporting information.** Moreover, the calculated adsorption capacities ($Q_{calc.}$) are very close to the experimental ones ($Q_{max.}$) values of SBA-15-OH adsorbent and the values of Q_{max} increase as the temperature increases indicating that the adsorption of GSH onto the SBA-15-OH adsorbent is favored at higher temperatures. In addition, the adsorption energy "b" of the SBA-15-OH adsorbent increased by increasing the solution temperature, indicating the higher affinity between the homogeneous active adsorption sites of the adsorbent and GSH [53].

One important parameter of the Langmuir isotherm model is the dimensionless constant, the separation factor (R_L). In this study, it was clear that the R_L values of SBA-15-OH and SBA-15-SH adsorbents were in the range 0-1 implying that the adsorption process is favorable, as discussed by Liou et *al.* [54].

3.5.Thermodynamics parameters

Thermodynamic parameters such as Gibb's free energy (ΔG°), enthalpy (ΔH°) and entropy (ΔS°) can be used to examine the energetic changes associated with the reaction

process. According to the adsorption studies, the Freundlich constant (K_F; **Table S2 in supporting information**) for SBA-15-NH_2 and the Langmuir constant or the adsorption energy constant (b; **Table S3 in supporting information**) for SBA-15-OH and SBA-15-SH have often been employed to calculate changes in Gibbs free energy according to the following **Eqs. (4)-(5)** [55]:

$$\Delta G° = \Delta H° - T\Delta S° = - R \times T \times \ln (K) \quad \textbf{(4)}$$

$$\ln(K) = \frac{\Delta S°}{R} - \frac{\Delta H°}{RT} \quad \textbf{(5)}$$

where K is b or K_F and R is the universal gas constant (8.314 $J.mol^{-1} K^{-1}$). The values of ΔH° and ΔS° were obtained from the slopes and the intercepts of the linear Van't Hoff plot, i.e ln(K) versus 1/T (**Figs. S8-S9 in supporting information**). The thermodynamic parameters are reported in **Table 4**.

Table 4. Thermodynamic parameters for the adsorption of GSH molecules onto SBA-15-OH, SBA-15-NH_2, and SBA-15-SH adsorbents.

Adsorbent	Temperature (K)	ΔG° ($kJ.mol^{-1}$)	ΔS° ($J.K^{-1}.mol^{-1}$)	ΔH° ($kJ.mol^{-1}$)
SBA-15-OH	283	-11.34±0.01	114.92±1.23	20.74±1.04
	295	-13.26±0.01		
	303	-13.73±0.01		
	313	-14.86±0.01		
SBA-15-NH_2	283	-4.32±0.01	63.71±0.44	13.54±0.23
	295	-5.55±0.01		
	303	-5.79±0.01		
	313	-6.25±0.01		
SBA-15-SH	283	-13.31±0.01	-54.44±0.365	-28.68±0.231
	295	-12.63±0.01		
	303	-12.06±0.01		
	313	-11.72±0.01		

The negative values of Gibbs free energy (ΔG°) whatever the temperature between from 283 and 313 K indicates that the reaction of GSH onto SBA-15-based adsorbents is spontaneous. As the temperature increases, the absolute values of ΔG° for the SBA-15-SH adsorbent decreases suggesting a decrease of the interactions between the adsorbent and the adsorbate molecules. For SBA-15-OH and SBA-15-NH_2 adsorbents, the ΔG° values become increasingly negative with increasing temperature, indicating that the reaction of GSH is favored with increasing temperature due to an increase in the mobility of GSH molecules to the active adsorption sites and a greater interaction between the adsorbate and the adsorbent surface [55]. On the other hand, the lower negative values of ΔG° of SBA-15-NH_2 when compared with those obtained for SBA-15-OH and SBA-15-SH, which also support that the elevated temperature would rise the adsorption capacity of GSH molecules. In addition, the ΔG° values reflects the nature of adsorption process. As discussed by Rodrigues et *al.*, [55] the adsorption nature can be classified as physisorption or chemisorption process when the values of ΔG° are in the range 0 to -20 $kJ.mol^{-1}$ and -80 and -400 $kJ.mol^{-1}$, respectively. Thus, the adsorption nature of the GSH molecules onto SBA-15-based adsorbents is a physical adsorption process. Additionally, the positive values of ΔH°, which were calculated to be 20.74±1.04 $kJ.mol^{-1}$ for SBA-15-OH and 13.54±0.23 $kJ.mol^{-1}$ for SBA-15-NH_2, showed the endothermic nature of the reaction process. The higher value of ΔH° for SBA-15-OH as compared to that of SBA-15-NH_2 showed that the GSH adsorption by SBA-15-OH required higher energy for the dehydration of the GSH molecules on the adsorbent surface during the adsorption process. In addition, the values of entropy (ΔS°) were calculated as 114.92±1.23 and 63.71±0.44 $J.mol^{-1}.K^{-1}$ for SBA-15-OH and SBA-15-NH_2, respectively. The positive values of entropy are related to the increase of the randomness at the adsorbent-solution interface during the adsorption process [56]. As a result of the use of the SBA-15-SH adsorbent, the negative value of ΔH°, indicating the exothermic nature of adsorption, and was explained by the decrease in adsorption capacity with

increasing temperature. Additionally, the obtained negative value of ΔS° for the SBA-15-SH adsorbent indicated that there might be a lower preference of GSH molecules for the adsorbent surface with the possibility of some structural change or the disorderliness in the complex SBA-15-SH/GSH during the adsorption process [57- 59].

4. Conclusion

In the present study, SBA-15 mesoporous materials were functionalized with 3-aminopropyltriethoxysilane (APTS) and (3-mercaptopropyl)triethoxysilane (MPTES) in order to introduce amine and thiol groups onto the surface by using a post-grafting method, respectively. Then, the SBA-15-based materials were used as adsorbents to further investigate the adsorption behavior of GSH under various experimental conditions. Among tested adsorbents, SBA-15-NH_2 showed the highest adsorption capacity (1.940±0.062 $mmol.g^{-1}$) under optimal experimental conditions ([GSH] = 10 $mg.mL^{-1}$, pH = 7 and T = 295 K). Moreover, to understand the mechanism of the adsorption kinetic process, pseudo-first order, pseudo-second order, Elovich, and Aharoni, models were fitted to experimental data. According to the adsorption data, the pseudo second-order and Aharoni models were suitable models to describe the adsorption of GSH molecules by SBA-15-NH_2 and SBA-15-SH adsorbents. Various adsorption isotherm models have also been evaluated. It was shown that the Langmuir isotherm model is the most appropriate one to simulate the adsorption of GSH molecules onto SBA-15-OH and SBA-15-SH adsorbents. The thermodynamic adsorption parameters were also evaluated and the obtained positive values for both enthalpy change (ΔH°) and entropy change (ΔS°) of SBA-15 and SBA-15-NH_2 adsorbents confirmed the endothermic features of the reaction process. On the contrary, the adsorption process was exothermic for the SBA-15-SH adsorption process.

Credit authorship contribution statement

Laroussi Chaabane: Conceived the research, designed the experiments, and draft the manuscript, **Maria Nikolantonaki:** Analyzed the data review and editing, **Guy Weber:** Investigation review and editing, **Igor Bezverkhyy:** Investigation review and editing, **Remi Chassagnon:** Software and data curation, **Ali Assifaoui:** Supervision, and project administrative, and **Frédéric Bouyer**: Supervision, Resources, writing review and editing. All authors discussed and revised the manuscript.

Declaration of Competing Interest

The authors declare that they have no known competing financial interests or personal relationships that could have appeared to influence the work reported in this paper.

Acknowledgements

The authors would like to express their gratitude to the Bourgogne Franche-Comté Region, the European funds FEDER, and the EUR EIPHI **(ANR-17-EURE-0002)** and the Valvigne project (**SYNERGIE BG0027582**) for their financial supports. We acknowledge Drs**. F. Herbst**, **N. Geoffroy** and **A. Krystianiak** for their advice in SEM, XRD and XPS characterization, respectively.

References

[1] Allison R B, Sacks G L, Brine-releasable hydrogen sulfide in wine: mechanism of release from copper complexes and effects of glutathione. J Agric Food Chem, 2021; 69: 13164-13172.

[2] Nikolantonaki M, Waterhouse A L A, Method to quantify quinone reaction rates with wine relevant nucleophiles: a key to the understanding of oxidative loss of varietal thiols. J Agric Food Chem 2012; 60: 8484-8491.

[3] Kritzinger E C F F, Bauer W J. Du Toit, Role of glutathione in winemaking: areview. J Agric Food Chem 2013; 61: 269-277.

[4] Li X, Ni T, Binding of glutathione and melatonin to pepsin occurs via different binding mechanisms. Eur Biophys J., 2016; 45: 165-174.

[5] Owen GW, Biologic and pharmacologic regulation of mammalian glutathione synthesis, Free Radic Biol Med 1999; 27: 922–935.

[6] Wang Q, Guan Y, Yang M, Application of superparamagnetic microspheres for affinity adsorption and purification of glutathione. J Magn Magn Mater 2012; 324: 3300-3305.

[7] Cheynier V, Souquet J M, Moutounet M, Glutathione content and glutathione to hydroxycinnamic acid ratio in Vitis vinifera grapes and musts. Am J Enol Vitic 1989; 40: 320-324.

[8] Wu X, Tang L, Du Y, Xu Z, Improving glutathione extraction from crude yeast extracts by optimizing aqueous two-phase system composition and operation conditions, Korean J Chem Eng, 2010; 271829-1835.

[9] Suzuki T, Yokoyama A, Tsuji T, Ikeshima E, Nakashima K, Ikushima S, Kobayashi C Yoshida S, Identification and characterization of genes involved in glutathione production in yeast. J Biosci Bioeng 2011; 112: 107-113.

[10] Carrera C, Ruiz-Rodríguez A, Palma M, Barroso C G, Ultrasound-assisted extraction of amino acids from grapes, Ultrason Sonochem 2015; 22: 499-505.

[11] Lorenz E, Schmacht M, Stahl U, Senz M, Enhanced incorporation yield of cysteine for glutathione overproduction by fed-batch fermentation of Saccharomyces cerevisiae, J. Biotechnol., 2015; 216: 131-139.

[12] Sasaki K, Hara K Y, Kawaguchi H, Sazuka T, Ogino C, Kondo A, Nanofiltration concentration of extracellular glutathione produced by engineered Saccharomyces cerevisiae. J. Biosci. Bioeng., 2016; 121: 96-100.

[13] Wang Y, Xiao T, Zhang Z, Feng X, Extraction and concentration of glutathione from yeast by membranes. Can J Chem Eng, 2022; 100: 195-204.

[14] Martínez J, García S, Alti L, Evaluation of glutathione content in white grape varieties. Vitis 2019; 58: 21-24.

[15] Hafezian S M, Biparva P, Bekhradnia A, Azizi S N, Amine and thiol functionalization of SBA-15 nanoparticles for highly efficient adsorption of sulforaphane. Adv Powder Technol 2021; 32: 779-790.

[16] Wang W, Wu G, Zhu T, Yang Y, Zhang Y, Synthesis of-thiazole Schiff base modified SBA-15 mesoporous silica for selective Pb (II) adsorption. J Taiwan Inst Chem Eng, 2021; 125: 349-359.

[17] Appaturi J N, Pulingam T, Rajabathar J R, Khoerunnisa F, Ling T C, Tan S H, Ng E P, Acid-base bifunctional SBA-15 as an active and selective catalyst for synthesis of ethyl α-cyanocinnamate via Knoevenagel condensation. Micropor. Mesopor. Mat., 2021; 320: 111091.

[18] Danesh-khorasgani M, Faghihian H, Givianrad M H, Aberoomand-Azar P, Saber-Tehrani M, Synthesis and application of a novel mesoporous SBA-15 sorbent functionalized by 2, 4

dinitrophenylhydrazine (DNPH) for simultaneous removal of Pb (II), Cr (III), Cd (II) and Co (II) from aqueous solutions: Experimental design, kinetic, thermodynamic, and isotherm aspects Adv Powder Technol 2022; 33: 103201.

[19] Ruchomski L, Pikula T, Kamiński D, Słowik G, Kosmulski M, Synthesis and characterization of novel composites derived from SBA-15 mesoporous silica and iron pentacarbonyl. J Colloid Interface Sci 2022; 608: 2421-2429.

[20] Kumar S, Malik M M, Purohit R, Synthesis methods of mesoporous silica materials 'Mater Today Proc 2017; 4A: 350-357.

[21] Soltani R, Shahvar A, Gordan H, Dinari M, Saraji M, Covalent triazine framework-decorated phenyl-functionalised SBA-15: its synthesis and application as a novel nanoporous adsorbent. New J Chem 2019; 43: 13058-13067.

[22] Zhao D, Feng J, Huo Q, Melosh N, Fredrickson G H, Chmelka B F, Stucky G D, Triblock copolymer syntheses of mesoporous silica with periodic 50 to 300 angstrom pores, Science 1998; 279: 548-552.

[23] Hernández-Morales V, Nava R, Acosta-Silva Y J, Macías-Sánchez S A, Pérez-Bueno J J B Pawelec, Adsorption of lead (II) on SBA-15 mesoporous molecular sieve functionalized with–NH2 groups, Micropor Mesopor Mat, 2012; 160: 133-142.

[24] Wu Y Q, Wei J W, Wang D Q, Removal of heavy metals in water by functionalized mesoporous silica materials: a review, J Adv Mater, 2013; 785: 693-696.

[25] Barczak M, Synthesis and structure of pyridine-functionalized mesoporous SBA-15 organosilicas and their application for sorption of diclofenac, J Solid State Chem, 2018; 258: 232-242.

[26] Liu F Y, Xiang M, Wang A, Wang C, Hu B. Efficient adsorption, and reduction of Cr (VI) and U (VI) by nanoscale zero-valent iron supported on polydopamine-decorated SBA-15. Appl. Surf Sci 2021; 568: 150931.

[27] Mahmoudi F, Amini M M, Sillanpää M. Hydrothermal synthesis of novel MIL-100 (Fe)@ SBA-15 composite material with high adsorption efficiency towards dye pollutants for wastewater remediation. J Taiwan Inst Chem Eng, 2020; 116: 303-313.

[28] Huang J, Ye M, Qu Y, Chu L, Chen R, He Q, Xu D, Pb (II) removal from aqueous media by EDTA-modified mesoporous silica SBA-15, J Colloid Interface Sci, 2012; 385: 137-146.

[29] Li J, Qi T, Wang L, Liu C, Zhang Y, Synthesipowder and characterization of imidazole-functionalized SBA-15 as an adsorbent of hexavalent chromium. Mater Lett, 2007; 61: 3197-3200.

[30] Jadhav S A, Miletto I, Brunella V, Berlier G, Scalarone D, Controlled postsynthesis grafting of thermoresponsive poly (Nisopropylacrylamide) on mesoporous silica nanoparticles. Polym Adv Technol, 2015; 26: 1070-1075.

[31] Zhao H, Han H, Synthesis, and characterization of functionalized SBA-15 silica through template removal, J Solid State Chem., 2020; 282: 121074.

[32] Costa J A S, de Jesus R A, Santos D O, Neris J B, Figueiredo R T, Paranhos C M, Synthesis, functionalization, and environmental application of silica-based mesoporous materials of the M41S and SBA-n families: a review J Environ Chem Eng, 2021; 9: 105259.

[33] Lee Y C, Lee D J, Cheng, C C, Zirconium involved platelet SBA-15: Synthesis and application to tannic acid adsorption. J Taiwan Inst Chem Eng, 2018; 93, 124-130.

[34] Dash S, Chaudhuri H, Gupta R, Nair U G, Adsorption study of modified coal fly ash with sulfonic acid as a potential adsorbent for the removal of toxic reactive dyes from aqueous solution: Kinetics and thermodynamics. J Environ Chem Eng 2018; 6: 5897-5905.

[35] Vavsari V F, Ziarani G M, Badiei A, The role of SBA-15 in drug delivery RSC Advances, 2015; 5: 91686-91707.

[36] Lashgari N, Badiei A, Ziarani G M, A novel functionalized nanoporous SBA-15 as a selective fluorescent sensor for the detection of multianalytes (Fe^{3+} and $Cr_2O_7^{2-}$) in water. J. Phys. Chem. Solids. 2017; 103: 238-248.

[37] Hassanzadeh-Afruzi F, Asgharnasl S, Mehraeen S, Amiri-Khamakani Z, Maleki A, Guanidinylated SBA-15/Fe_3O_4 mesoporous nanocomposite as an efficient catalyst for the synthesis of pyranopyrazole derivatives. Sci Rep 2021; 11: 19852.

[38] Nguyen C H, Fu C C, Chen Z H, Van Tran T T, Liu S H, Juang R S, Enhanced and selective adsorption of urea and creatinine on amine-functionalized mesoporous silica SBA-15 via hydrogen bonding Micropor Mesopor Mat, 2021; 311: 110733.

[39] Moritz M, Geszke-Moritz M, Sulfonic acid derivative-modified SBA-15, PHTS and MCM-41 mesoporous silicas as carriers for a new antiplatelet drug: Ticagrelor adsorption and release Studies. Materials, 2020; 13: 2913.

[40] Yuan P, Li X, Wang W, Liu H, Yan Y, Yang H, Yue Y, Bao X, Tailored design of differently modified mesoporous materials to deeply understand the adsorption mechanism for polycyclic aromatic hydrocarbons. Langmuir, 2018; 34: 15708-15718.

[41] Chaabane L, Beyou E, El Ghali A, Baouab M H V, Comparative studies on the adsorption of metal ions from aqueous solutions using various functionalized graphene oxide sheets as supported adsorbents, J Hazard Mater, 2020; 389: 121839.

[42] Li Y, Sun N, Li L, Zhao N, Xiao F, Wei W, Sun Y, Huang W, Grafting of amines on ethanol-extracted SBA-15 for CO_2 adsorption, Materials, 2013; 6: 981-999.

[43] Abid Z, Hakiki A, Boukoussa B, Launay F, Hamaizi H, Bengueddach A, Hamacha R, Preparation of highly hydrophilic PVA/SBA-15 composite materials and their adsorption behavior toward cationic dye: effect of PVA content, J Mater Sci, 2019; 54: 7679–7691.

[44] Li Q, Wang Z, Fang D M, Qu H Y, Zhu Y, Zou H J, Chen Y R, Du Y P, Hu H L, Preparation, characterization, and highly effective mercury adsorption of l-cysteine-functionalized mesoporous silica, New J Chem, 2014; 38: 248-254.

[45] Shahraki S, Delarami H S, Khosravi F, Nejat R, Improving the adsorption potential of chitosan for heavy metal ions using aromatic ring-rich derivatives, J Colloid Interface Sci, 2020; 576: 79-89.

[46] Shen C, Chen C, Wen T, Zhao Z, Wang X, Xu A, Superior adsorption capacity of g-C_3N_4 for heavy metal ions from aqueous solutions, J Colloid Interface Sci, 2015; 456: 7-14.

[47] Chaabane L, Beyou E, Luneau D, Baouab M H V, Functionalization of graphene oxide sheets with magnetite nanoparticles for the adsorption of copper ions and investigation of its potential catalytic activity toward the homocoupling of alkynes under green conditions, J Catal 2020: 388; 91-103.

[48] Aharoni C, Sideman S, Hoffer E, Adsorption of phosphate ions by collodion- coated

[49] Liu H, Zhang X, Hou L, Zheng H, Niu B, Weng K, Fu J, Nitrogen-rich hierarchical porous polyphosphazene for rapid and efficient adsorption of anionic contaminants: Kinetics, isotherm, thermodynamics and mechanism, Appl Surf Sci, 2023: 616; 156538.

[50] Knight A W, Tigges A B, Ilgen A G, Adsorption of copper (II) on mesoporous silica: the effect of nano-scale confinement. Geochem. Trans, 2018: 19; 1-13.

[51] Ayawei N, Ebelegi A N, Wankasi D, Modelling and interpretation of adsorption isotherms, J Chem 2017: 2017; 1-11.

[52] Ragadhita R, Nandiyanto A B D, How to calculate adsorption isotherms of particles using two-parameter monolayer adsorption models and equations. Indones. J Sci Technol 2021: 6; 205-234.

[53] Bernal V, Giraldo L., Moreno-Piraján J C, Physicochemical Parameters of the Methylparaben Adsorption from Aqueous Solution Onto Activated Carbon and Their Relationship with the Surface Chemistry. ACS Omega, 2021: 6; 8797-8807.

[54] Liou T H, Chen G W, Yang S, Preparation of Amino-Functionalized Mesoporous SBA-15 Nanoparticles and the Improved Adsorption of Tannic Acid in Wastewater. Nanomaterials, 2022:12; 791.

[55] Rodrigues L A, Pinto da Silva M L C, Alvarez-Mendes M O, Coutinho A d R, Thima, G P, Phenol removal from aqueous solution by activated carbon produced from avocado kernel seeds, Chem. Eng. J. 2011: 174; 49–57.

[56] Chaabane L, Beyou E, Baouab M H V, Preparation of a novel zwitterionic graphene oxide-based adsorbent to remove of heavy metal ions from water: Modeling and comparative studies. Adv Powder Technol, 2021: 32; 2502-2516.

[57] Nasiri-Ardali M, Nezamzadeh-Ejhieh A, A comprehensive study on the kinetics and thermodynamic aspects of batch and column removal of Pb(II) by the clinoptilolite–glycine adsorbent, Mater Chem Phys, 2020, 240: 122142.

[58] Isah U, Abdulraheem G, Bala S, Muhammad S, Abdullahi M, Kinetics, equilibrium and thermodynamics studies of CI Reactive Blue 19 dye adsorption on coconut shell based activated carbon. Int Biodeterior Biodegrad, 2015; 102: 265-273.

[59] Bardajee G R, Hooshyar Z, Shahidi F E, Synthesis, and characterization of a novel Schiff-base/SBA-15 nanoadsorbent for removal of methylene blue from aqueous solutions, Int J Environ Sci Technol, 2015; 12: 1737-1748.